



1 **Along-stream transport and transformation of dissolved organic**

2 **matter in a large tropical river**

3

4 Thibault Lambert^{1,*}, Cristian R. Teodoru², Frank C. Nyoni³, Steven Bouillon², François

5 Darchambeau¹, Philippe Massicotte⁴ and Alberto V. Borges¹.

6

7

8 ¹ University of Liège, Chemical Oceanography Unit, Liège, Belgium

9 ² KU Leuven, Department of Earth and Environmental Sciences, Leuven, Belgium

10 ³ University of Zambia, Integrated Water Resources Management Center, Lusaka,

11 Zambia

12 ⁴ Aarhus University, Department of Bioscience, Denmark

13 * Corresponding author

14

15

16

17

18

19

20

21



Abstract - Large rivers transport considerable amounts of terrestrial dissolved organic matter (DOM) to the ocean. Yet, downstream gradients and temporal variability in DOM fluxes and characteristics are poorly studied at the scale of large river basins, especially in tropical areas. Here, we report longitudinal patterns in DOM content and composition based on absorbance and fluorescence measurements along the Zambezi River and its main tributary, the Kafue River, during two hydrological seasons. During high flow periods, a greater proportion of aromatic and humic DOM was mobilized along rivers due to the hydrological connectivity with wetlands and high flow velocities, while low flow periods were characterized by lower DOM content of less aromaticity resulting from loss of connectivity with wetlands, more efficient degradation of terrestrial DOM and enhanced autochthonous productivity. Changes in water residence time due to contrasting water discharge were found to modulate the fate of DOM along the river continuum. Thus, terrestrial DOM dynamics shifted from transport-dominated during the wet seasons towards degradation during the dry season, with substantial consequences on longitudinal DOM content and composition. The longitudinal evolution of DOM was also strongly impacted by a hydrological buffering effect in large reservoirs in which the seasonal variability of DOM fluxes and composition was strongly reduced.



22 1. Introduction

23 The composition, transport and transformation of dissolved organic matter (DOM)
24 in large rivers are key aspects for determining regional and global carbon (C) budgets
25 (Schlesinger and Melack, 1981), the fate of terrigenous DOM flowing to the oceans (del
26 Giorgio and Pace, 2008; Massicotte and Frenette, 2011), the influence of fluvial inputs on
27 DOM biogeochemistry in coastal and oceanic environments (Holmes et al., 2008), and
28 the functioning of inland waters as active pipes with regards to the global C cycle (Cole et
29 al., 2007; Borges et al., 2015a). Riverine DOM is mainly derived from terrestrial soils (e.g.
30 Weyhenmeyer et al., 2012), but can also be fueled by sources within the aquatic system
31 (Lapierre and Frenette, 2009; Massicotte and Frenette, 2011). Longitudinal patterns of
32 riverine DOM, both in terms of concentration and composition, are controlled by numerous
33 environmental drivers including connectivity with surrounding wetlands (Battin, 1998;
34 Mladenov et al., 2007), lateral inputs from tributaries (Massicotte and Frenette, 2011) and
35 shifts in dominant land cover (Ward et al., 2015). Once in the aquatic ecosystem, terrestrial
36 DOM is exposed to in-stream processing such as photodegradation (Cory et al., 2007;
37 Spencer et al., 2009), microbial respiration (Amon and Benner, 1996; Fasching et al.,
38 2014), and flocculation (von Wachenfeldt and Tranvik, 2008), that usually operate
39 simultaneously and lead to the removal and the transformation of DOM during its transport
40 (Massicotte and Frenette, 2011; Cawley et al., 2012). The overall reactivity of DOM in
41 freshwater is largely controlled by its composition (Kothawala et al., 2014; Kellerman et
42 al., 2015). For example, the selective loss of the colored fraction of terrestrial DOM is a
43 common pattern observed in a wide variety of ecosystems (Moran et al., 2000; Cory et al.,
44 2007; Spencer et al., 2009; Weyhenmeyer et al., 2012). However, the extent of DOM
45 decay depends on the water residence time (WRT) of the aquatic ecosystem (Cory et al.,



46 2007; Hanson et al., 2011; Köhler et al., 2013). In large rivers, WRT varies spatially,
47 increasing in reservoirs and lakes compared to river channels, and seasonally, being
48 higher during low flow compared to high flow. Considering that changes in water level also
49 control the hydrological connectivity with wetlands, it is likely that the downstream gradient
50 in DOM composition drastically differs in relation to spatial and temporal changes in
51 hydrodynamic conditions.

52 Longitudinal patterns of DOM in large rivers are often assessed in one specific
53 environment, such as wetlands/floodplains (Mladenov et al., 2007; Yamashita et al., 2010;
54 Cawley et al., 2012; Zurbrügg et al., 2013) or lakes (Parks and Baker, 1997; Massicotte
55 and Frenette 2013; Stackpoole et al., 2014), or limited to a subsection of large rivers (del
56 Giorgio and Pace; 2008; Massicotte and Frenette, 2011; Ward et al., 2015), and mostly
57 carried out during one specific hydrological period. Our understanding of rivers as a
58 continuum in which DOM is simultaneously transported from terrestrial soils to oceans,
59 produced and degraded is thus fundamentally limited by a lack of basin-scale studies
60 taking into account seasonal variations. This is especially true for tropical waters that have
61 the highest riverine dissolved organic carbon (DOC) flux to the oceans (Meybeck, 1993)
62 but for which DOM cycling has received less attention than rivers in other biomes with the
63 exception of the Amazon River (Mayorga et al., 2005; Johnson et al., 2011; Ward et al.,
64 2013; 2015).

65 The study of DOM biogeochemistry at large spatial and temporal scales requires
66 analytical tools that are simple to implement but have a large sample throughput while
67 providing pertinent information about the DOM chemical composition. Spectroscopic
68 methods, primarily based on ultraviolet-visible and fluorescence measurements, fulfill
69 these criteria (Jaffé et al., 2008). Optical properties of colored DOM (CDOM) and



70 fluorescent DOM (FDOM) can be used to calculate several indices related to DOM
71 composition. These include the specific ultra violet absorbance at 254 nm (SUVA₂₅₄),
72 positively related to the degree of DOM aromaticity (Weishaar et al., 2003), the spectral
73 slope ratio (S_R), inversely related to the average DOM molecular weight (Helms et al.,
74 2008) and the fluorescence index (FI), related to the contribution of terrestrial versus
75 microbial inputs (McKnight et al., 2001). FDOM measurements acquired as three-
76 dimensional excitation-emission matrices (EEMs) and coupled with the parallel factor
77 analysis (PARAFAC) provide additional benefits for the characterization of DOM
78 (Stedmon et al., 2003; Stedmon and Markager, 2005; Yamashita et al., 2008). In addition,
79 the carbon stable isotope composition of DOC ($\delta^{13}\text{C}_{\text{DOC}}$) can provide information about
80 the terrestrial or aquatic origin of DOM (Mladenov et al., 2007; Lambert et al., 2015).

81 The Zambezi River basin, the fourth largest river in Africa, was extensively sampled
82 from its source to its mouth during three field campaigns carried out over wet and dry
83 seasons (Teodoru et al., 2015; Fig. 1 and 2). Longitudinal patterns of DOM were assessed
84 through measurements of DOC concentrations and characterization of DOM ($\delta^{13}\text{C}_{\text{DOC}}$
85 coupled with CDOM and FDOM) along the Zambezi River (>3000 km) and its main
86 tributary, the Kafue River (>1500 km). The aim of this study was to determine the main
87 drivers on downstream patterns of DOM at the scale of a large tropical river, with a specific
88 attention for the role of WRT in modulating the fate of DOM.

89 **2. Materials and methods**

90 **2.1. Study site.** The Zambezi River has a drainage area of 1.4×10^6 km², originates in
91 northwest Zambia and flows southeast over 3000 km before it discharges into the Indian
92 Ocean in Mozambique (Fig. 1). The climate of the Zambezi Basin is classified as humid



93 subtropical and is characterized by two main seasons, the rainy season from
94 October/November to April/May and the dry season from May/June to
95 September/October. Annual precipitation strongly varies with latitude, from > 2000 mm in
96 the northern part and around Lake Malawi to less than 500 mm in the southern part of the
97 basin. The mean annual rainfall over the entire catchment is ~940 mm (Chenje, 2000). Up
98 to 95% of the annual rainfall occurs during the rainy period while the dry period presents
99 irregular and sporadic rainfall events. Consequently, water discharge in Zambezi River
100 has a bimodal distribution with a single maximum peak discharge occurring typically in
101 April/May and a minimum in November (Fig. 2).

102 Woodlands and shrublands are the dominant (55%) land cover and stretch over the
103 whole catchment, forests (20%) and grasslands (9%) areas are mainly confined to the
104 northeast part of the basin and croplands represents 13% of the total area (Mayaux et al.,
105 2004). Wetlands, including swamps, marshes, seasonally inundated floodplains and
106 mangroves cover 5% of the total basin area (Lehner and Döll, 2004).

107 Based on distinct geomorphological characteristics, the Zambezi Basin can be divided
108 into three major segments: (1) the upper Zambezi from the headwaters to Victoria Falls;
109 (2) the middle Zambezi, from Victoria Falls to the edge of the Mozambique coastal plain
110 (below Cahora Bassa Gorge); and (3) the lower Zambezi, the stretch crossing the coastal
111 plain down to the Indian Ocean (Wellington, 1955). The upper Zambezi covers about 40%
112 of the total area of the Zambezi basin but comprises the highest fraction of wetlands and
113 floodplains (about 60% of the total wetlands/floodplains areas of the Zambezi Basin),
114 including the Barotse Floodplain and the Chobe Swamps (Fig. 1). The middle stretch of
115 the Zambezi River is buffered by two major man-made impoundments, namely the Kariba
116 Reservoir (volume: 157 km³; area: 5364 km²) and the Cahora Bassa Reservoir (volume:



117 63 km³; area: 2739 km²). The Kafue River (drainage area: 1.56×10^5 km²) joins the
118 Zambezi River ~ 70 km downstream of the Kariba Dam. Similarly to the upper Zambezi,
119 the Kafue River comprises a high density of wetlands/floodplains (about 26% of the total
120 wetlands/floodplains areas of the Zambezi basin), including the Lukanga Swamps and the
121 Kafue Flats (Fig. 1). It also comprises two smaller reservoirs, the Itezhi Tezhi Reservoir
122 (volume: ~ 6 km³; area: 365 km²) and the Kafue Gorge Reservoir (volume: ~1 km³; area:
123 13 km²). In its lower part, the Zambezi River and its tributary the Shire River both drain
124 narrow but ~ 200 km long wetlands areas before their confluence zone. At the end of its
125 course, the river forms a large, 100 km long floodplain-delta system of swamps and
126 meandering channels.

127 **2.2. Sampling and analytical methods.** Sampling was conducted during two
128 consecutive years and over two climatic seasons: wet season (1 February to 5 May, n=40)
129 2012, wet season (6 January to 21 March, n=41) 2013, and dry season (15 October to 28
130 November, n=24) 2013 (Fig. 2). Sites in the Zambezi and the Kafue rivers were located
131 100 – 150 km apart from the spring to the outlet (Fig. 1) except during the 2013 dry season
132 when sampling in the Zambezi River ended before its entrance in the Cahora Bassa
133 Reservoir due to logistical constraints.

134 Water sampling was mainly performed from boats or dugout canoes in the middle
135 of the river. In few case (n=10), in the absence of boats/canoes, sampling was carried out
136 either from bridges or directly from the shore and as far as possible away from the
137 shoreline, but without discernable effects on the longitudinal patterns on DOM or other
138 biogeochemical variables (Teodoru et al., 2015). Approximately 2 L of water were
139 collected 0.5 m below the surface, kept away from direct sunshine and filtered and
140 conditioned within 2 h of sampling. Filtrations were performed successively on pre-



141 combusted GF/F glass fiber filters (0.7 μm porosity), then on 0.2 μm polyethersulfone
142 syringe filters. Samples for the measurement of DOC concentration and $\delta^{13}\text{C}_{\text{DOC}}$
143 signatures were stored in 40 mL glass vials with polytetrafluoroethylene (PTFE) coated
144 septa with 50 μL H_3PO_4 (85%). Samples for CDOM/FDOM analyses were stored in 20 mL
145 amber glass vials with PTFE-coated septa but without H_3PO_4 addition. Samples for major
146 elements (including Fe) were stored in 20 mL scintillation vials and acidified with 50 μl of
147 HNO_3 65 % prior to analysis.

148 **2.3. DOC analysis.** DOC and $\delta^{13}\text{C}_{\text{DOC}}$ were analyzed with an Aurora1030 total organic
149 carbon analyzer (OI Analytical) coupled to a Delta V Advantage isotope ratio mass
150 spectrometer. Typical reproducibility observed in duplicate samples was in most cases <
151 ± 5 % for DOC, and ± 0.2 ‰ for $\delta^{13}\text{C}_{\text{DOC}}$. Quantification and calibration was performed
152 with an aqueous solution of IAEA-C6 and in-house sucrose standards.

153 **2.4. CDOM analysis and calculations.** Absorbance was recorded on a Perkin-Elmer
154 UV/Vis 650S spectrophotometer using a 1 cm quartz cuvette. Absorbance spectra were
155 measured between 190 and 900 nm at 1 nm increment and instrument noise was
156 assessed measuring ultrapure (Type 1) Milli-Q (Millipore) water as blank. After subtracting
157 the blank spectrum, the correction for scattering and index of refraction was performed by
158 fitting the absorption spectra to the data over the 200-700 nm range according to the
159 following equation:

$$160 \quad A_{\lambda} = A_0 e^{-S(\lambda-\lambda_0)} + K \quad (1)$$

161 where A_{λ} and A_0 are the absorbance measured at defined wavelength λ and at reference
162 wavelength $\lambda_0 = 375$ nm, respectively, S the spectral slope (nm^{-1}) that describes the
163 approximate exponential decline in absorption with increasing wavelength and K a



164 background offset. The fit was not used for any purpose other than to provide an offset
165 value K that was then subtracted from the whole spectrum (Lambert et al., 2015).

166 The $SUVA_{254}$ was calculated as the UV absorbance at $\lambda = 254$ nm (A_{254}) normalized
167 to the corresponding DOC concentration (Weishaar et al., 2003). The natural UV
168 absorbance of Fe at $\lambda = 254$ nm was estimated based on measured Fe concentrations
169 and was then subtracted from the UV absorbance measured. The corrected value of A_{254}
170 was then used to calculate $SUVA_{254}$. The $SUVA_{254}$ was used as an indicator of the
171 aromaticity of DOC with high values (>3.5 l $mgC^{-1} m^{-1}$) indicating the presence of more
172 complex aromatic moieties and low values (<3 l $mgC^{-1} m^{-1}$) indicative the presence of
173 mainly hydrophobic compounds (Weishaar et al., 2003).

174 Napierian absorption coefficients were calculated according to:

$$175 \quad a_{\lambda} = 2.303 \times A_{\lambda}/L \quad (3)$$

176 where a_{λ} is the absorption coefficient (m^{-1}) at wavelength λ , A_{λ} the absorbance corrected
177 at wavelength λ and L the path length of the optical cell in m (0.01 m). CDOM was reported
178 as the absorption coefficient at 350 nm (a_{350}). Spectral slopes for the intervals 275-295
179 nm and 350-400 nm were determined from the linear regression of the log-transformed a
180 spectra versus wavelength. The slope ratio S_R was calculated as the ratio of $S_{275-295}$ to
181 $S_{350-400}$ according to Helms et al. (2008). S_R is related to the molecular weight distribution
182 of DOM with values less than 1 indicative of enrichment in high molecular weight
183 compounds and high values above 1 indicative of a high degree of low molecular weight
184 compounds (Helms et al., 2008).

185 **2.5. FDOM analysis and PARAFAC modeling.** Fluorescence intensity was recorded on
186 a Perkin-Elmer LS55 fluorescence spectrometer using a 1 cm quartz cuvette across
187 excitation wavelengths of 220-450 nm (5 nm increments) and emission wavelengths of



188 230-600 nm (0.5 nm increments) in order to build excitation–emission matrices (EEMs). If
189 necessary, samples were diluted until $A_{254} < 0.2 \text{ m}^{-1}$ to avoid problematic inner filter effects
190 (Ohno, 2002). Before each measurement session (i.e. each day), a Milli-Q water sample
191 was also analysed. EEMs preprocessing such as removing first and second Raman
192 scattering, standardization to Raman units, absorbance corrections and inner filter effects
193 were performed prior the PARAFAC modelling. The scans were standardized to Raman's
194 units (normalized to the integral of the Raman signal between 390 nm and 410 nm in
195 emission at a fixed excitation of 350 nm) with a Milli-Q water sample run the same day as
196 the samples (Zepp et al., 2004). PARAFAC model was using MATLAB (MathWorks,
197 Natick, MA, USA) and DOM Fluorescence Toolbox 1.7. PARAFAC model was validated
198 by split-half analysis and random initialization (Stedmon and Bro, 2008). Additional
199 samples analysed in the same manner and collected from (1) tributaries of the Zambezi
200 and the Kafue rivers as well as during a two-years monitoring period of the Zambezi and
201 the Kafue rivers ($n = 42$; data not published), and (2) the Congo Basin ($n = 164$; data not
202 published) were added to the dataset. This was done to increase the variability of DOM
203 fluorescence signatures and therefore help detect components that could have been
204 present in insufficient quantity to be detected in our environment (Stedmon and Markager,
205 2005). The maximum fluorescence F_{Max} values of each component for a particular sample
206 provided by the model were summed to calculate the total fluorescence signal F_{Tot} of the
207 sample in Raman's unit (R.U.). The relative abundance of any particular PARAFAC
208 component X was then calculated as $\%C_X = F_{\text{Max}}(X) / F_{\text{Tot}}$. The FI index was calculated as
209 the ratio of the emission intensities at 470 nm and 520 nm at an excitation wavelength of
210 370 nm (McKnight et al., 2001). A higher FI value (e.g., 1.8) indicates a microbial DOM



211 source while a lower value (e.g., 1.2) indicates a terrestrial source; intermediate values
212 indicate a mixed DOM source.

213 **2.6. Statistical Analysis**

214 PCA was performed on scaled variables using the `prcomp` function in R software. DOC
215 concentrations, stable carbon isotopic composition, optical indices ($SUVA_{254}$, S_R , FI), a_{350} ,
216 F_{Max} and the relative abundance of PARAFAC components were used as the variables for
217 the PCA. Given the different units of the variables used in the PCA, data were scaled to
218 zero-mean and unit-variance as recommended (Borcard et al., 2011). The PCA was then
219 performed on the correlation matrix of the scaled variables.

220 **3. Results**

221 **3.1. Longitudinal patterns in DOC concentration, composition and DOM optical** 222 **properties**

223 Data were acquired during two wet seasons and one dry season, the two wet
224 seasons data are discussed together hereafter. DOC concentrations in the Zambezi River
225 ranged from 1.9 ± 0.1 to 4.9 ± 1.0 mg L⁻¹ during the wet periods and from 1.2 to 2.9 mg L⁻
226 ¹ and the dry period (Fig. 3A). Along the upper Zambezi DOC increased downstream
227 during the wet seasons, while DOC gradually decreased downstream during the dry
228 season. In the Kariba Reservoir, DOC variability between wet and dry seasons was
229 relatively low, and concentrations ranged from 2.4 ± 0.3 to 2.9 ± 1.4 mg L⁻¹. DOC exhibited
230 relatively small variability downstream of the Kariba Reservoir and along the lower
231 Zambezi, with the exception of a slight increase during the wet seasons downstream of
232 the confluence with the Shire River (outlet of Lake Malawi).



233 In the Kafue River, DOC was generally higher during the wet seasons (from $3.1 \pm$
234 0.1 to 5.4 ± 0.7 mg L⁻¹) compared to the dry season (from 1.3 to 3.6 mg L⁻¹)(Fig. 3B).
235 Despite this seasonal difference, DOC increased gradually downstream during both wet
236 and dry seasons. DOC concentrations in the Itezhi Tezhi Reservoir showed a decrease
237 (~25%) during the wet seasons but an increase (~20%) during the dry season compared
238 to the upstream station.

239 The a_{350} values (Fig. 3C and 3D) were higher during the wet seasons (1.7 to 16.6
240 m⁻¹ in the Zambezi and 3.9 to 11.5 m⁻¹ in the Kafue) than during the dry season (1.3 to
241 10.7 m⁻¹ in the Zambezi and 1.2 to 4.7 m⁻¹ in the Kafue). They followed similar spatial and
242 seasonal patterns as DOC concentrations, with some differences. First, decreases in a_{350}
243 values were more pronounced than for DOC, especially in the upper Zambezi during the
244 dry season and in the Kariba and Itezhi Tezhi reservoirs during the wet season. For
245 example, while DOC decreased by a factor ~2 as the Zambezi enters the Kariba Reservoir
246 during the wet periods, a_{350} decreased by a factor ~4. Secondly, while DOC
247 concentrations were higher at the outlet of reservoirs compared to upstream stations
248 during the dry season, a_{350} values were lower.

249 $\delta^{13}\text{C}_{\text{DOC}}$ showed a gradual increase along the Zambezi River during all periods
250 from -28.1 and -26.5 ‰ at the source to -21.4 to -20.1 ‰ near its delta, the latter being
251 especially marked between the two first sampling sites in the upper Zambezi (Fig. 3E),
252 while no significant pattern was observed along the Kafue River (values between -25.9
253 and -20.5 ‰, Fig. 3F).

254 DOM at the source of the Zambezi exhibited the highest SUVA_{254} (> 4 L mgC⁻¹ m⁻¹)
255 and lowest S_R (< 0.8) values during both wet and dry seasons (Fig. 3G and 3I). During
256 the wet seasons, the upper Zambezi was characterized by stable SUVA_{254} ($3.5 - 4.0$ L



257 $\text{mgC}^{-1} \text{m}^{-1}$) and low S_R (0.85 – 0.91) values. In the middle Zambezi, $SUVA_{254}$ and S_R
258 values were lowest ($2.2 \pm 0.2 - 2.9 \pm 0.1 \text{ L mgC}^{-1} \text{m}^{-1}$) and highest ($1.22 \pm 0.09 - 1.41 \pm$
259 0.01) in the Kariba and the Cahora Bassa reservoirs compared to samples collected in-
260 between ($2.6 \pm 0.1 - 3.1 \pm 0.02 \text{ L mgC}^{-1} \text{m}^{-1}$ for $SUVA_{254}$ and $0.97 \pm 0.1 - 1.10 \pm 0.08$ for
261 S_R). Overall, $SUVA_{254}$ increased from 2.1 ± 0.5 to $2.9 \pm 0.9 \text{ L mgC}^{-1} \text{m}^{-1}$ whereas S_R
262 decreased from 1.08 ± 0.09 to 0.97 ± 0.04 in the lower Zambezi, with a maximum (3.3 ± 0.9
263 $\text{L mgC}^{-1} \text{m}^{-1}$) and a minimum (0.88 ± 0.006) values recorded below the confluence with the
264 Shire River, respectively. During the wet periods, FI values ranged between 1.24 and 1.41
265 in the mainstream, and between 1.43 and 1.58 in reservoirs (Fig. 3K). FI values during
266 the dry season were globally higher than during the wet periods with values ranging from
267 1.29 to 1.72, except at the source of the Zambezi, where an FI value of 1.19 was observed.

268 In the Kafue River, variations in DOM composition were marked between the wet
269 and dry seasons, but minimal along the longitudinal transect (Fig. 3H, 3J and 3L). $SUVA_{254}$
270 and S_R ranged from 3.5 to 4.0 $\text{L mgC}^{-1} \text{m}^{-1}$ and from 0.79 to 1.05, respectively, during the
271 wet seasons, except in the Itezhi Tezhi Reservoir where $SUVA_{254}$ decreased to 2.4 L mgC^{-1}
272 m^{-1} and S_R increased up to 1.16. Values were quite stable during dry periods, and ranged
273 between 2.2 and 2.8 $\text{L mgC}^{-1} \text{m}^{-1}$ for $SUVA_{254}$ and from 1.11 to 1.22 for S_R . FI values
274 ranged between 1.27 and 1.42 during the wet seasons, and between 1.41 and 1.74 during
275 the dry season.

276 3.2. Longitudinal patterns in FDOM

277 PARAFAC modelling identified three terrestrial humic-like components (C1, C2 and
278 C4), one microbial humic-like component (C3) and one protein tryptophan-like (C5)
279 component (Table 1 and Supplementary Fig. 1). In the Zambezi River, the fluorescence
280 intensities (F_{Max}) of PARAFAC components during the wet seasons presented patterns



281 similar to DOC concentrations with some exceptions (Fig. 4). The increase of F_{Max} for the
282 C4 component (calculated as the percentage of increase between lowest and highest
283 values recorded in corresponding river sections, data not shown) was higher than for the
284 other components in river sections draining wetlands/floodplains in the upper and lower
285 Zambezi. All terrestrial and microbial humic-like components showed a systematic and
286 marked decrease in their F_{Max} values in reservoirs, while F_{Max} of C5 decreased in a smaller
287 proportion in the Kariba Reservoir and increased in the Cahora Bassa Reservoir. During
288 the dry season, F_{Max} of terrestrial humic-like components decreased downstream as DOC
289 concentrations, while F_{Max} remained stable for C3 or increased for C5. In the Kafue River,
290 F_{Max} of all components followed similar spatial and temporal patterns as those of DOC
291 concentrations. The main difference observed was that while F_{Max} values of humic-like
292 compounds were lower during the dry season compared to the wet seasons, F_{Max} of C5
293 exhibited similar values across the hydrological cycle.

294 As a direct consequence of the spatial and temporal differences in F_{Max} of
295 PARAFAC components, the relative contribution of each component to the total
296 fluorescence signal F_{TOT} showed distinct patterns (Fig. 5). Thus, the downstream
297 decrease of %C1 and %C2 observed in the upper Zambezi during the wet seasons can
298 be related to the parallel increase of %C4, the latter being due to the more pronounced
299 increase in F_{Max} of C4 relative to the other components. The same patterns for %C1 and
300 %C2 observed during the dry season, however, reflect the fact that F_{Max} values of C3 and
301 C5 were stable or increased during the dry season, respectively, while F_{Max} of C1 and C2
302 decreased. %C5 was higher during the dry season compared to the wet seasons, and
303 reached highest values in reservoirs during the wet periods due to its specific spatial and
304 temporal variations in F_{Max} values. No longitudinal changes in the relative abundance of



305 PARAFAC components were observed along the Kafue River. Similar to what was
306 observed along the Zambezi River, the dry season was marked by a decrease in %C4
307 and an increase in %C5, while %C1, %C2 and %C3 were equivalent to values recorded
308 during the wet seasons.

309 **3.3. Principal component analysis (PCA)**

310 The first two components of the PCA explained 71.7% of the variance and
311 regrouped the variables in three main clusters (Fig. 6). The first includes %C1, %C2 and
312 samples collected at or near the source of the Zambezi. The second group was defined
313 by %C4 and several variables including DOC, F_{Max} , $SUVA_{254}$ and a_{350} . Samples from the
314 upper Zambezi and from the Kafue rivers (excluding reservoirs) were mainly located in
315 this cluster. Finally, %C3 and %C5 were clustered with S_R and FI. Samples from reservoirs
316 (including Kariba, Cahora Bassa and Itezhi Tezhi) were almost all in this cluster. Samples
317 from the middle and lower Zambezi collected during the wet seasons and those collected
318 during the dry season were located between the distinct clusters defined by PARAFAC
319 components and other variables.

320 **4. Discussion**

321 **4.1. Identification of PARAFAC components.** Humic-like components C1 and C2 are
322 among the most common fluorophores found in freshwaters and are associated with high
323 molecular weight and aromatic compounds of terrestrial origin (Stedmon and Markager,
324 2005; Yamashita et al., 2008; Walker et al., 2013). Component C4 has been reported to
325 be of terrestrial origin (Stedmon and Markager, 2005; Kothawala et al., 2015) or to be a
326 photoproduct of terrestrially derived DOM (Massicotte and Frenette, 2011). The
327 association of %C4 with DOC concentrations and terrestrial optical indices including a_{350}



328 and $SUVA_{254}$ advocates for a terrestrial origin of this component (Fig. 6). Inversely, %C3
329 and %C5 were negatively correlated with a_{350} and $SUVA_{254}$. C3 and C5 components are
330 respectively classified as microbial humic-like and tryptophan-like components related to
331 the production of DOM within aquatic ecosystems (Kothawala et al., 2014; Kellerman et
332 al., 2015). Both fluorophores can originate from autochthonous primary production
333 (Yamashita et al., 2008; 2010; Lapierre and Frenette, 2009) or from degradation of
334 terrestrial DOM in the water column as previously reported in a wide variety of
335 environments as marine (Jørgensen et al., 2011) and lake waters (Kellerman et al., 2015)
336 for C3, and large Arctic rivers (Walker et al., 2013) or small temperate catchment (Stedmon
337 and Markager, 2005) for C5. The opposite relationship of %C1 and %C2 versus %C3 (Fig.
338 6) suggests that C3 would be the result of the transformation of terrestrial components C1
339 and C2 through biological activity in the water column as suggested by Jørgensen et al.
340 (2011). The distribution of samples along PC1 is thus likely controlled by the transition
341 from terrestrial DOM with a high degree of aromaticity and humic content (negative
342 loadings) to less aromatic DOM produced within the aquatic ecosystem by the degradation
343 of terrestrial DOM during transport and/or by autochthonous sources (positive loadings).

344 **4.2. Seasonal and spatial variability in downstream gradients in DOM concentration**
345 **and composition.** Altogether data showed clear changes in the downstream gradients of
346 DOM concentration and composition, both seasonally and spatially. These changes were
347 essentially controlled by three main factors: WRT and connectivity with
348 wetlands/floodplains, both highly dependent on seasonal variations of water level (and
349 discharge), and water retention by lakes/reservoirs that is more independent from
350 seasonal variations of water level. Dominant land cover was also found to affect DOM
351 gradients, but to a lesser degree.



352 **4.2.1 Land cover and hydrological connectivity with wetlands/floodplains.** The DOM
353 at the source of the Zambezi was clearly distinct from the rest of the basin, independently
354 of the hydrological period (Fig. 6), with a strong aromatic character (highest $SUVA_{254}$), a
355 high degree of molecules with elevated molecular weight (lowest S_R) and low $\delta^{13}C_{DOC}$.
356 The dominant land cover quickly shifts from forest in the northern part of the basin where
357 the Zambezi takes its source to grassland and woodland/shrubland that dominate in the
358 rest of the basin (Supplementary Fig. 2). This shift in land cover was reflected in the DOM
359 gradient from the source station of the Zambezi to the next sampling site, and marked by
360 an increase in S_R , $\delta^{13}C_{DOC}$ and a decrease in $SUVA_{254}$. This pattern is consistent with the
361 role of forest in releasing more aromatic DOM of high molecular weight than other
362 vegetation types in tropical freshwaters (Lambert et al., 2015).

363 Downstream, the variability in the optical properties of DOM between wet and dry
364 seasons indicated seasonal changes in the sources of riverine DOM in relation with
365 changes in water level and connectivity with wetlands/floodplains. The high $SUVA_{254}$ and
366 low S_R values during the wet seasons indicate the mobilisation of fresh aromatic DOM of
367 high molecular weight due to the increased water flow through DOM-rich upper soil
368 horizons during high flow periods (Striegl et al., 2005; Neff et al., 2006; Mann et al., 2012;
369 Bouillon et al., 2014). Wetlands and floodplains were the main sources of terrestrial DOM
370 at the basin scale during wet seasons, as shown by the relationships between DOC and
371 wetland extent (Fig. 7). Among the different terrestrial humic-like components, C4 was the
372 most affected by fluctuations in the connectivity with wetlands/floodplains. The increase
373 in the relative contribution of C4 suggests that this component was mobilized in greater
374 proportion relative to others (Fig. 5). This observation is consistent with a recent study
375 conducted in boreal streams, in which a component similar to C4 was found to increase



376 relative to other humic-like fluorophores (equivalent to C1 and C2) in stream waters during
377 the peak spring melt due to the higher abundance of this component in uppermost soil
378 horizons of wetlands (Kothawala et al., 2015). The longitudinal and seasonal variations in
379 %C4 in the upper Zambezi are consistent with the hypothesis that C4 is mainly produced
380 in the upper soil horizons of wetlands/floodplains and therefore preferentially mobilized
381 during high flow periods.

382 **4.2.2 WRT modulates the downstream patterns of DOM.** During the dry season, DOM
383 was characterized by lower SUVA₂₅₄ and higher S_R values, indicating the transport of
384 compounds of lower aromaticity and lower average molecular weight compared to high
385 flow periods. The difference in downstream gradients of DOM compared to the wet
386 seasons can be explained in part by the loss of connectivity between rivers and riparian
387 wetlands/floodplains and the deepening of hydrological flowpaths through DOM-poor
388 deeper subsoil horizons during the dry season (e.g. Striegl et al., 2005; Bouillon et al.,
389 2014). Changes of connectivity with wetland during the dry season was also found to
390 strongly impact CO₂ and CH₄ distribution in the Zambezi (Teodoru et al., 2015). That being
391 said, the considerable decrease in water discharge during dry/base flow period compared
392 to wet/high flow periods (Fig. 2) likely leads to a decrease in water velocities and
393 subsequently to an increase in solutes residence time, allowing a more efficient
394 degradation of terrestrial DOM along a given section. For illustration, the preferential
395 downstream loss of a₃₅₀ compared to DOC in the upper Zambezi, associated with a
396 gradual decrease of SUVA₂₅₄ and increase of S_R, is a strong evidence of the preferential
397 loss of the terrestrial and aromatic fraction of DOM through photodegradation (e.g.
398 Spencer et al., 2009; Weyhenmeyer et al., 2012). The stable level of F_{Max} of C3 suggests
399 a continuous supply of this component, likely due to microbial degradation of terrestrial



400 DOM. In addition, the increase in WRT could favour the accumulation of DOM from
401 autochthonous sources as suggested by higher values of FI and the gradual increase in
402 F_{Max} for C5 (Fig. 3 and 4). Flushing during high flow periods perturbs the downstream
403 gradient of DOM established during base flow because (1) increase in water level
404 mobilizes a greater proportion of terrestrial DOM and (2) increase in water velocities
405 increases the travel distance of humic and aromatic terrestrial compounds before removal
406 due to microbial and photochemical degradation processes and limits the accumulation of
407 autochthonous DOM in the water column.

408 **4.2.3. Retention of water by lakes/reservoirs.** Longitudinal patterns of DOM were
409 affected by the presence of reservoirs independently of water level fluctuations, in which
410 DOM was characterized by low aromaticity and molecular weight and higher microbial
411 contribution (Fig. 4 and 6). The net loss of DOC and the preferential loss of the coloured
412 and aromatic fraction of DOM (based on a_{350} and $SUVA_{254}$, Fig. 3) in lakes and reservoirs
413 have been previously documented (Hanson et al., 2011; Köhler et al., 2013) and attributed
414 to the combination of several processes including flocculation, photochemical and
415 microbial degradation (Cory et al., 2007; von Wachenfeldt and Tranvik, 2008; Köhler et
416 al., 2013; Kothawala et al., 2014). Although we were not able to estimate the relative
417 contribution of these mechanisms, our results indicate that the humic-like fractions of DOM
418 (C1-C4) were more susceptible to degradation compared to the protein-like fraction (C5),
419 an observation consistent with recent studies carried out in boreal lakes (Kothawala et al.,
420 2014). The level of fluorescence of C5 could be additionally sustained by the FDOM from
421 primary producers such as macrophytes (Lapierre and Frenette, 2009), that also lead to
422 low values of the partial pressure of CO_2 in the Kariba and Cahora Bassa reservoirs
423 (Teodoru et al., 2015).



424 In agreement with others studies (e.g. Hanson et al., 2011), the effects of reservoirs
425 on the fate of DOM were related to their specific WRT. The Itezhi Tezhi Reservoir had
426 little effect on longitudinal patterns of DOM, as also suggested by a recent study (Zürbrugg
427 et al., 2013), likely due to its relatively low WRT (0.7 yr, Kunz et al., 2011) compared to
428 the Kariba (5.7 yr, Magadza, 2010) and the Cahora Bassa (~2 yr, Davies et al., 2000)
429 reservoirs. The DOC concentrations upstream and downstream of the Cahora Bassa
430 Reservoir were similar but DOM composition exhibited significant changes within the
431 reservoir compared to upstream and downstream stations, suggesting a balance between
432 loss and production of new compounds. In fact, the Kariba Reservoir was the most
433 important reservoir responsible for the perturbation of the longitudinal DOM gradient. The
434 seasonal variability of DOM at the outlet of the Kariba Reservoir, both in terms of
435 concentration and composition, was drastically reduced compared to the seasonal
436 patterns observed in the upper Zambezi (Fig. 3 and 5). This was also illustrated by data
437 from a two-years monitoring of the Zambezi River 70 km downstream of the Kariba Dam,
438 showing that the terrestrial fraction of DOM leaving the reservoir has undergone extensive
439 transformation (Table 2).

440 Beyond their role as hotspots for DOM processing and mineralization,
441 lakes/reservoirs act as a hydrological buffer and reduce the temporal variability of
442 downstream water flow (Goodman et al., 2011; Lottig et al. 2013). Except for some
443 isolated events, water discharge remained constant at Kariba Dam due to hydropower
444 management (Fig. 2). Combined with the low temporal variability in DOM content (Table
445 2), DOC fluxes at the outlet of the Kariba Reservoir were relatively invariant and ranged
446 between 8.3×10^7 and 9.7×10^7 kg yr⁻¹. This results in a twofold decrease of DOC fluxes



447 during the wet seasons between upstream inputs from the upper Zambezi and export at
448 the outlet of the Kariba Reservoir, but in the increase by a factor of 12 during the dry
449 season (Fig. 8). On a longitudinal perspective, lakes/reservoirs can thus shift from DOM
450 source to sink relative to upstream ecosystems while reducing the temporal variation of
451 DOM fluxes and composition to downstream ecosystems. That being said, DOM losses
452 were largely offset during the wet seasons by inputs from the Kafue and the Shire rivers
453 as well as from wetlands in the lower Zambezi (Fig. 3 and 8). Therefore, the spatial
454 arrangement of the different elements that constitute large river networks such as
455 lakes/reservoirs, wetlands/floodplains and large tributaries is a key aspect in controlling
456 DOM export at the basin scale.

457 **4.3. Comparison with others rivers.** The results of this study are similar to those
458 reported in large rivers from other biomes regarding (1) the role of peak flow periods in
459 exporting a greater portion of terrestrial aromatic and humic DOM (Neff et al., 2006; Duan
460 et al., 2007; Holmes et al., 2008; Walker et al., 2013), (2) the disproportionate importance
461 of riparian wetlands and floodplains in regulating in-stream chemistry (Battin, 1998;
462 Hanley et al., 2013; Borges et al., 2015b) and (3) the reactivity of terrestrial DOM during
463 its transport (Massicotte and Frenette, 2011; Cawley et al., 2012; Wehenmeyer et al.,
464 2012). However, while changes in temperature have been suggested as a secondary
465 factor impacting DOM patterns in temperate and boreal streams and rivers (Kothawala et
466 al., 2014; Raymond et al., 2015), changes in longitudinal DOM patterns in the Zambezi
467 Basin were only controlled by changes in hydrology. Indeed, water temperatures were
468 systematically elevated with values mainly ranging from 25 to 29°C (data not shown) and
469 no significant patterns were apparent between the contrasting seasons.



470 Our study clearly illustrates that the DOC in a given station is the legacy of
471 upstream sources and their degree of processing during transport, and suggests that WRT
472 is a major driver controlling the fate of DOM in freshwaters (the latter resulting from the
473 competition between transport and degradation processes). Seasonal changes in DOM
474 concentration and composition in large rivers assessed by monitoring programs are often
475 explained by vertical changes in DOM sources mobilized during high flow and base flow
476 conditions, i.e. shallow versus deep sources along the soil profile (Neff et al., 2006; Mann
477 et al., 2012; Bouillon et al., 2014). Our results show that the upstream degradation history
478 of DOM during transit should also be taken into consideration, especially during base flow
479 periods. Given the strong reactivity of fresh terrestrial humic DOM exported during high
480 flow periods (e.g. Holmes et al., 2008; Mann et al., 2012) and the ability of large
481 hydrological events to transport DOM downstream over large distances (Raymond et al.,
482 2015), the functioning of large rivers at the seasonal scale and their impacts on receiving
483 ecosystems (e.g. coastal waters) should deserve more attention.

484

485 **Author contributions**

486 The research project was designed by AVB and SB, field data collection was done by
487 CRT and FCN. CDOM and FDOM measurements were done by TL with the help of FD.
488 Data analysis was done by TL with the help of PM for PARAFAC modelling. Manuscript
489 was drafted by TL that was commented, amended and approved by all co-authors.

490 **Acknowledgements**

491 This work was funded by the European Research Council (ERC-StG 240002 AFRIVAL),
492 the Fonds National de la Recherche Scientifique (FNRS, FluoDOM J.0009.15), the



493 Research Foundation Flanders (FWO-Vlaanderen), the Research Council of the KU
494 Leuven. We thank Christiane Lancelot (Université Libre de Bruxelles) for access to the
495 Perkin-Elmer UV/Vis 650S. TL is a postdoctoral researcher at the FNRS. AVB is a senior
496 research associate at the FNRS.

497 **Supplementary Information** accompanies this paper.

498

499 **References**

- 500 Amon, R. M. W. and Benner, R.: Bacterial utilization of different size classes of dissolved
501 organic matter, *Limnol. Oceanogr.*, 41, 41–51, 1996.
- 502 Battin, T. J.: Dissolved organic matter and its optical properties in a blackwater tributary
503 of the upper Oricono river, Venezuela, *Org. Geochem.*, 28, 561-569, 1998.
- 504 Borcard, D., Gillet, F., and Legendre, P.: *Numerical ecology with R*, Springer New York,
505 New York, 306 pp., doi.org/10.1007/978-1-4419-7976-6, 2011.
- 506 Borges, A. V., Darchambeau, F., Teodoru, C. R., Marwick, T. R., Tamooch, F.,
507 Geeraert, N., Omengo, F. O., Guerin, F., Lambert, T., Morana, C., Okuku, E.,
508 and Bouillon, S.: Globally significant greenhouse-gas emissions from african
509 inland waters, *Nature Geosci.*, doi:10.1038/ngeo2486, 2015a.
- 510 Borges, A. V., Abril, G., Darchambeau, F., Teodoru, C. R., Deborde, J., Vidal, L. O.,
511 Lambert, T., and Bouillon, S.: Divergent biophysical controls of aquatic CO₂ and CH₄
512 in the World's two largest rivers; *Sci. Rep.*, 5, 15614, doi: 10.1038/srep15614, 2015b.
- 513 Bouillon, S., Yambélé, A., Gillikin, D. P., Teodoru, C. R., Darchambeau, F., Lambert, T.,
514 and Borges, A. V.: Contrasting biogeochemical characteristics of the Oubangui River



- 515 and tributaries (Congo River basin), *Sci. Rep.*, 4, 1–10, doi:10.1038/srep05402,
516 2014.
- 517 Cawley, K. M., Wolski, P., Mladenov, N., and Jaffé, R.: Dissolved organic matter
518 biogeochemistry along a transect of the Okavango delta, Botswana, *Wetlands*, 32,
519 475–486, doi: 10.1007/s13157-012-0281-0, 2012.
- 520 Chenje, M.: *State of the Environment Zambezi Basin 2000*, SADC, IUCN, ZRA, and
521 SARDC, Maseru, Lusaka and Harare, 334 pp., ISBN 978-1-77910-009-2, 2000.
- 522 Cole, J. J., Prairie, Y. T., Caraco, N. F., McDowell, W. H., Tranvik, L. J., Striegl, R. G.,
523 Duarte, C. M., Kortelainen, P., Downing, J. A., Middelburg, J. J., and Melack, J.:
524 Plumbing the global carbon cycle: integrating inland waters into the terrestrial carbon
525 budget, *Ecosystems*, 10, 171–184, 2007.
- 526 Cory, R. M., McKnight, D. M., Chin, Y. P., Miller, P., and Jaros, C. L.: Chemical
527 characteristics of fulvic acids from Arctic surface waters: Microbial contributions and
528 photochemical transformations, *J. Geophys. Res.-Biogeosci.*, 112, G04S51,
529 doi:10.1029/2006JG000343, 2007.
- 530 Davies, B. R., Beilfuss, R. D., and Thoms, M. C.: Cahora Bassa retrospective, 1974-1997:
531 effects of flow regulation on the lower Zambezi River, *Verh. Int. Ver. Theor. Angew.*,
532 20, 2149–2157, 2000.
- 533 del Giorgio, P. A. and Pace, M. L.: Relative independence of dissolved organic carbon
534 transport and processing in a large temperate river: the Hudson River as both pipe
535 and reactor, *Limnol. Oceanogr.*, 53, 185-197, 2008.
- 536 Duan, S., Bianchi, T. and Sampere, T. P.: Temporal variability in the composition and
537 abundance of terrestrially-derived dissolved organic matter in the lower Mississippi



- 538 and Pearl Rivers, *Mar. Chem.*, 103, 172–184, doi:10.1016/j.marchem.2006.07.003,
539 2007.
- 540 Fasching, C., Behounek, B., Singer, G. A., and Battin, T. J.: Microbial degradation of
541 terrigenous dissolved organic matter and potential consequences for carbon cycling
542 in brown-water streams, *Scientific reports*, 4, doi:10.1038/srep04981, 2014.
- 543 Goodman, K. J., Baker, M. A., and Wurtsbaugh, W. A.: Lakes as buffers of stream
544 dissolved organic matter (DOM) variability: temporal patterns of DOM characteristics
545 in mountain stream-lake systems, *J. Geophys. Res.*, 116, G00N02,
546 doi:10.1029/2011JG001709, 2011.
- 547 Hanley, K., Wollheim, W. M., Salisbury, J., Huntington, T., and Aiken, G.: Controls on
548 dissolved organic carbon quantity and chemical character in temperate rivers of
549 North America, *Global Biogeochem. Cycles*, 27, 492–504, doi:10.1002/gbc.20044,
550 2013.
- 551 Hanson, P. C., Hamilton, D. P., Stanley, E. H., Preston, N., Langman, O. C., and Kara, E.
552 L.: Fate of allochthonous dissolved organic carbon in lakes: a quantitative approach,
553 *PLoS ONE*, 6, e21884, doi:10.1371/journal.pone.0021884, 2011.
- 554 Helms, J. R., Stubbins, A., Ritchie, J. D., Minor, E. C., Kieber, D. J., and Mopper, K.:
555 Absorption spectral slopes and slope ratios as indicators of molecular weight,
556 source, and photobleaching of chromophoric dissolved organic matter, *Limnol.*
557 *Oceanogr.*, 53, 955–969, 2008.
- 558 Holmes, R. M., McClelland, J. W., Raymond, P. A., Frazer, B. B., Peterson, B. J., and
559 Stieglitz, M.: Lability of DOC transported by Alaskan rivers to the arctic ocean,
560 *Geophys. Res. Lett.*, 35, 5, L03402, doi:10.1029/2007gl032837, 2008.



- 561 Jaffé, R., McKnight, D., Maie, N., Cory, R., McDowell, W. H., and Campbell, J. L.: Spatial
562 and temporal variations in DOM composition in ecosystems: The importance of long-
563 term monitoring of optical properties, *J. Geophys. Res.-Biogeo.*, 113, G04032,
564 doi:10.1029/2008jg000683, 2008.
- 565 Johnson, M S., Couto, E. G. Abdo, M., and Lehmann, J.: Fluorescence index as an
566 indicator of dissolved organic carbon quality in hydrologic flowpaths of forested
567 tropical watersheds, *Biogeochemistry*, 105, 149-157, doi: 10.1007/s10533-011-
568 9595-x, 2011.
- 569 Jørgensen, L., Stedmon, C. A., Kragh, T., Markager, S., Middelboe, M., and Søndergaard,
570 M.: Global trends in the fluorescence characteristics and distribution of marine
571 dissolved organic matter, *Mar. Chem.*, 126, 139–148, doi:
572 10.1016/j.marchem.2011.05.002, 2011.
- 573 Kellerman, A. M., Kothawala, D. N., Dittmar, T., and Tranvik, L. J.: Persistence of
574 dissolved organic matter in lakes related to its molecular characteristics, *Nat.*
575 *Geosci.*, 8, 454–457, doi: 10.1038/ngeo2440, 2015.
- 576 Köhler, S. J., Kothawala, D., Futter, M. N., Liungman, O., and Tranvik, L.: In-lake
577 processes offset increased terrestrial inputs of dissolved organic carbon and color in
578 lakes, *PLoS ONE*, 8, e70598, doi:10.1371/journal.pone.0070598, 2013.
- 579 Kothawala, D. N., Ji, X., Laudon, H., Ågren, A., Futter, M. N., Köhler, S. J., and Tranvik,
580 L. J.: The relative influence of land cover, hydrology, and in-stream processing on
581 the composition of dissolved organic matter in boreal streams, *J. Geophys. Res.-*
582 *Biogeo.*, 120, 1491–1505, doi: 10.1002/2015JG002946, 2015.
- 583 Kothawala, D. N., Stedmon, C. A., Müller, R. A., Weyhenmeyer, G. A., Köhler, S. J., and
584 Tranvik, L. J.: Controls of dissolved organic matter quality: Evidence from a large-



- 585 scale boreal lake survey, *Glob. Change Biol.*, 20, 1101–1114,
586 doi:10.1111/gcb.12488, 2014.
- 587 Kunz, M. J., Wuest, A., Wehrli, B., Landert, J., and Senn, D. B.: Impact of a large tropical
588 reservoir on riverine transport of sediment, carbon and nutrients to downstream
589 wetlands, *Water Resour. Res.*, 47, W12531, doi:10.1029/2011WR010996, 2011.
- 590 Lambert, T., Darchambeau, F., Bouillon, S., Alhou, B., Mbega, J- D, Teodoru, C. R., Nyoni,
591 F. C., and A V Borges, A. V.: Landscape control on the spatial and temporal
592 variability of chromophoric dissolved organic matter and dissolved organic carbon in
593 large African rivers, *Ecosystems*, 18, 1224–1239, doi:10.1007/s10021-015-9894-5,
594 2015.
- 595 Lapierre, J. F. and Frenette, J. J.: Effects of macrophytes and terrestrial inputs on
596 fluorescent dissolved organic matter in a large river system, *Aquat. Sci.*, 71, 15–24,
597 doi:10.1007/s00027-009-9133-2, 2009.
- 598 Lehner, B. and Döll, P.: Development and validation of a global database of lakes,
599 reservoirs and wetlands, *J. Hydrol.*, 296, 1–22, doi:10.1016/j.jhydrol.2004.03.028,
600 2004.
- 601 Lottig, N. R., Buffam, I., and Stanley, E. H.: Comparisons of wetland and drainage lake
602 influences on stream dissolved organic concentrations and yields in a north
603 temperate lake-rich region, *Aquat. Sci.*, 75, 619–630, doi: 10.1007/s00027-013-
604 0305-8, 2013.
- 605 Magadza, C.: Environmental state of Lake Kariba and Zambezi River Valley: Lessons
606 learned and not learned. *Lakes & Reservoirs: Research & Management*, 15, 167–
607 192, doi:10.1111/j.1440-1770.2010.00438.x, 2010.



- 608 Mann, P. J., Davydova, A., Zimov, N., Spencer, R. G. M., Davydov, S., Bulygina, E.,
609 Zimov, S. and Holmes, R. M.: Controls on the composition and lability of dissolved
610 organic matter in Siberia's Kolyma River basin, *J. Geophys. Res.*, 117, G01028,
611 doi:10.1029/2011JG001798, 2012.
- 612 Massicotte, P. and Frenette, J.-J.: Spatial connectivity in a large river system: resolving
613 the sources and fate of dissolved organic matter, *Ecol. Appl.*, 21, 2600–2617, 2011.
- 614 Mayaux, P., Bartholomé, E., Fritz, S., and Belward, A.: A new land-cover map of Africa for
615 the year 2000, *J. Biogeogr.*, 31, 861–877, 2004.
- 616 Mayorga, E., Aufdenkampe, A. K., Masiello, C. A., Krusche, A. V., Hedges, J. I., Quay, P.
617 D., Richey, J. E., and Brown, T. A.: Young organic matter as a source of carbon
618 dioxide outgassing from Amazonian rivers, *Nature*, 436, 538–541,
619 doi:10.1038/nature03880, 2005.
- 620 McKnight, D. M., Boyer, E. W., Westerhoff, P. K., Doran, P. T., Kulbe, T., and Andersen,
621 D. T.: Spectrofluorometric characterization of dissolved organic matter for indication
622 of precursor organic material and aromaticity, *Limnol. Oceanogr.*, 46, 38–48, 2001.
- 623 Meybeck, M.: Riverine transport of atmospheric carbon: source, global typology and
624 budget. *Water, Air, and Soil Pollution*, 70, 443–463, 1993.
- 625 Mladenov, N, McKnight, D. M., Macko, S. A., Norris, M., Cory, R. M., and Ramberg, L.:
626 Chemical characterization of DOM in channels of a seasonal wetland, *Aquat. Sci.*,
627 69, 456–471, doi:10.1007/s00027-007-0905-2, 2007.
- 628 Moran, M. A., Sheldon, W. M., and Zepp, R. G.: Carbon loss and optical property changes
629 during long-term photochemical and biological degradation of estuarine dissolved
630 organic matter, *Limnol. Oceanogr.*, 45, 1254–1264, 2000.



- 631 Neff, J. C., Finlay, J. C., Zimov, S. A., Davydov, S. P., Carrasco, J. J., Schuur, E. A. G.,
632 and Davydova, A. I.: Seasonal changes in the age and structure of dissolved organic
633 carbon in Siberian rivers and streams *Geophys. Res. Lett.*, 33, L23401,
634 doi:10.1029/2006GL028222, 2006.
- 635 Ohno, T.: Fluorescence inner-filtering correction for determining the humification index of
636 dissolved organic matter, *Environ. Sci. Technol.*, 36, 742–746,
637 doi:10.1021/Es0155276, 2002.
- 638 Parks, S. J. and Baker, L. A.: Sources and transport of organic carbon in an Arizona river-
639 reservoir system, *Wat. Res.*, 31, 1751–1759, 1997.
- 640 Raymond, P. A., Saiers, J. E., and Sobczak W. V.: Hydrological and biogeochemical
641 controls on watershed dissolved organic matter transport: pulse-shunt concept,
642 *Ecology*, in press, doi.org/10.1890/14-1684.1, 2015.
- 643 Schlesinger, W. H. and Melack, J. M.: Transport of organic carbon in the world's rivers,
644 *Tellus*, 33, 172-187, 1981.
- 645 Spencer, R. G. M., Stubbins, A., Hernes, P. J., Baker, A., Mopper, K., Aufdenkampe, A.
646 K., Dyda, R. Y., Mwamba, V. L., Mangangu, A. M., Wabakanghanzi, J. N., and Six,
647 J.: Photochemical degradation of dissolved organic matter and dissolved lignin
648 phenols from the Congo River, *J. Geophys. Res.-Biogeo.*, 114,
649 doi:10.1029/2009jg000968, 2009.
- 650 Stackpoole, S. M., Stets, E. G., and Striegl, R. G.: The impact of climate and reservoirs
651 on longitudinal riverine carbon fluxes from two major watersheds in the Central and
652 Intermontane West, *J. Geophys. Res.-Biogeo.*, 119, 848–863, doi:
653 10.1002/2013JG002496, 2014.



- 654 Stedmon, C. A. and Markager, S.: Resolving the variability in DOM fluorescence in a
655 temperate estuary and its catchment using PARAFAC, *Limnol. Oceanogr.*, 50, 686–
656 697, 2005.
- 657 Stedmon, C. A. and Bro, R.: Characterizing dissolved organic matter fluorescence with
658 parallel factor analysis: a tutorial, *Limnol. Oceanogr. Meth.*, 6, 572–579, 2008.
- 659 Stedmon, C. A., Markager, S., and Bro, R.: Tracing dissolved organic matter in aquatic
660 environments using a new approach to fluorescence spectroscopy, *Mar. Chem.*, 82,
661 239–254, doi:10.1016/s0304-4203(03)00072-0, 2003.
- 662 Striegl, R. S., Aiken, G. R., Domblaser, M. M., Raymond, P. A., and Wickland, K. P.: A
663 decrease in discharge-normalized DOC export by the Yukon River during summer
664 through autumn, *Geophys. Res. Lett.*, 32, L21413, doi:10.1029/2005GL024413,
665 2005.
- 666 Teodoru, C. R., Nyoni, F. C., Borges, A. V., Darchambeau, F., Nyambe, I., and Bouillon,
667 S.: Dynamics of greenhouse gases (CO₂, CH₄, N₂O) along the Zambezi River and
668 major tributaries, and their importance in the riverine carbon budget,
669 *Biogeosciences*, 12, 2431–2453, doi:10.5194/bg-12-2431-2015, 2015.
- 670 von Wachenfeldt, E. and Tranvik, L. J.: Sedimentation in Boreal lakes - the role of
671 flocculation of allochthonous dissolved organic matter in the water column.
672 *Ecosystems* 11, 803–814, doi: 10.1007/s10021-008-9162-z, 2008.
- 673 Walker, S. A., Amon, R. M., and Stedmon, C. A.: Variations in high-latitude riverine
674 fluorescent dissolved organic matter: A comparison of large Arctic rivers, *J.*
675 *Geophys. Res.-Biogeophys.*, 118, 1689–1702, doi:10.1002/2013JG002320, 2013.
- 676 Ward, N. D., Keil, R. G., Medeiros, P. M., Brito, D. C., Cunha, A. C., Dittmar, T., Yager, P.
677 L., Krusche, A. V., and Richey, J. E.: Degradation of terrestrially derived



- 678 macromolecules in the Amazon River, *Nat. Geosci.*, 6, 530–533,
679 doi:10.1038/ngeo1817, 2013.
- 680 Ward, N. D., Krusche, A. V., Sawakuchi, H. O., Brito, D. C., Cunha, A. C., Moura, J. M.
681 S., da Silva, R., Keil, R. G., and Richey, J. E.: The compositional evolution of
682 dissolved and particulate organic matter along the lower Amazon River-Óbidos to
683 the ocean, *Mar. Chem.*, 177, 244–256, doi.org/10.1016/j.marchem.2015.06.013,
684 2015.
- 685 Weishaar, J. L., Aiken, G. R., Bergamaschi, B. A., Fram, M. S., Fujii, R., and Mopper, K.:
686 Evaluation of specific ultraviolet absorbance as an indicator of the chemical
687 composition and reactivity of dissolved organic carbon, *Environ. Sci. Technol.*, 37,
688 4702–4708, doi: 10.1021/es030360x, 2003.
- 689 Wellington, J. H.: *Southern Africa – a Geographic Study*, vol. 1, *Physical Geography*,
690 Cambridge University Press, Cambridge, 528 pp., 1955.
- 691 Weyhenmeyer, G. A., Fröberg, M., Karlton, E., Khalili, M., Kothawala, D., Temnerud, J.,
692 and Tranvik, L. J.: Selective decay of terrestrial organic carbon during transport from
693 land to sea, *Glob. Change Biol.*, 18, 349–355, doi:10.1111/j.1365-
694 2486.2011.02544.x, 2012.
- 695 Yamashita, Y., Jaffé, R., Maie, N. and Tanoue, E.: Assessing the dynamics of dissolved
696 organic matter (DOM) in coastal environments by excitation emission matrix
697 fluorescence and parallel factor analysis (EEM-PARAFAC), *Limnol. Oceanogr.*, 53,
698 1900–1908, 2008.
- 699 Yamashita, Y., Scinto, L. J., Maie, N., and Jaffé, R.: Dissolved organic matter
700 characteristics across a subtropical wetland's landscape: application of optical



701 properties in the assessment of environmental dynamics, *Ecosystems*, 13, 1006–
702 1019, doi:10.1007/s10021-010-9370-1, 2010.

703 Zepp, R. G., Sheldon, W. M., and Moran, M. A.: Dissolved organic fluorophores in
704 southeastern US coastal waters: correction method for eliminating Rayleigh and
705 Raman scattering peaks in excitation–emission matrices, *Mar. Chem.*, 89, 15–36,
706 doi:10.1016/j.marchem.2004.02.006, 2004.

707 Zurbrügg, R., Suter, S., Lehmann, M. F., Wehrli, B., and Senn, D. B.: Organic carbon and
708 nitrogen export from a tropical dam-impacted floodplain system, *Biogeosciences*, 10,
709 23–38, doi: 10.5194/bg-10-23-2013, 2013.

710

711 **Figure captions**

712 **Figure 1** – Map of the Zambezi basin illustrating the digital elevation model, wetlands and
713 floodplains areas (data from Lehner and Döll, 2004), the main hydrological network and
714 the distribution of sampling sites along the Zambezi and the Kafue rivers.

715 **Figure 2** – Water discharge between January 2012 and January 2014 for (a) the Zambezi
716 River at Victoria Falls and at Kariba Dam, and (b) for the Kafue River at Hook Bridge
717 located upstream of the Itezhi Tezhi Reservoir and at the Kafue Gorge Dam (data from
718 Zambia Electricity Supply Corporation Limited, ZESCO). Bars refer to the three periods
719 during which field campaigns were performed.

720 **Figure 3** – Longitudinal variations of DOM properties along the Zambezi River (left panels)
721 and the Kafue River (right panels) during the wet and the dry seasons. From top to bottom
722 the panels represent: DOC, a_{350} , $\delta^{13}\text{C}_{\text{DOC}}$, SUVA_{254} , S_{R} and FI. Dark gray and light gray
723 rectangles in background represent the approximate position along the mainstream of



724 wetlands/floodplains areas and reservoirs, respectively. Roman numerals refer to (I)
725 Barotse Floodplain, (II) Chobe Swamps, (III) Kariba Reservoir, (IV) Cahora Bassa
726 Reservoir, (V) lower Zambezi wetlands for the Zambezi River and (VI) Lukanga Swamps,
727 (VII) Itezhi Tezhi Reservoir and (VIII) Kafue Flats for the Kafue River. The diamonds
728 represent samples collected from main tributaries upstream to their confluence with
729 mainstreams: (IX) the Kabompo, (X) the Kafue, (XI) the Luangwa, (XII) the Mazoe and
730 (XIII) Shire River for the Zambezi River and (XIV) the Lunga River for the Kafue River.
731 Symbols and error bars for data collected during the wet seasons represent the average
732 and standard deviation between the two field campaigns performed in 2012 and 2013,
733 respectively.

734

735 **Figure 4** – Longitudinal variations of FDOM along the Zambezi River (left panels) and the
736 Kafue River (right panels) during the wet and the dry seasons. From top to bottom the
737 panels represent: F_{Tot} and F_{Max} for each PARAFAC component. The diamonds represent
738 samples taken from main tributaries upstream their confluence with mainstreams.

739

740 **Figure 5** – Longitudinal variations of the relative contribution of PARAFAC component
741 along the Zambezi River (left panels) and the Kafue River (right panels) during the wet
742 and the dry seasons. The diamonds represent samples taken from main tributaries
743 upstream their confluence with mainstreams.

744

745 **Figure 6** – Graphical representation of PCA results, including loadings plot for the input
746 variables and scores plot for water samples collected during the wet dry (circles) and the
747 wet (triangles) seasons. Water samples from the Zambezi River (ZBZ) were classified



748 according to its source and the three major segments of the Zambezi basin. Samples from
749 reservoirs (i.e. Kariba, Cahora Bassa and Itezhi Tezhi reservoirs) were classified together.

750

751 **Figure 7** – Relationships between DOC and % Wetlands in the Zambezi and the Kafue
752 rivers, with *:p<0.1, and ***:p<0.001.

753

754 **Figure 8** – DOC fluxes calculated at different locations along the Zambezi River during
755 the wet and the dry seasons. Vertical arrows represent changes in DOC fluxes at a same
756 location between the wet and the dry seasons. Diagonal changes represent longitudinal
757 variations.



758 **Table 1**– Spectral characteristics of the five fluorophores identified by PARAFAC modelling, correspondence with previously
 759 identified components in different environments, general assignment and possible source. Numbers in brackets refer to the
 760 second peak of maximal excitation.

Component	Maximum Excitation (nm)	Maximum Emission (nm)	Comparison with others environments								Assignment	Possible source ^a
			St Lawrence River ¹	Large Arctic rivers ²	Boreal Lakes ^{3,4}	Subtropical wetlands ^{5,6}	Tropical wetland ⁷	Temperate estuary ⁸	Coastal waters ⁹	Marine waters ¹⁰		
C1	<240 (325)	443	C2	C1	C4	C1	C1	C4	—	C1	Terrestrial humic-like	T
C2	<240 (365)	517	C3	C3	C3	C5	C4	C2	C3	—	Terrestrial humic-like	T
C3	<240 (305)	383	C7	—	C2	C4	C3	C6	C6	C4	Microbial humic-like	Au ⁹ , M ^{6,7,10} , An ⁸
C4	<240	405	C1	—	C5	C2	C2	C1	C1	—	Terrestrial humic-like	T ^{5-6,8} , P ^{1,4}
C5	275 (<240)	337	C4	C5	C6	C8	—	C7	C4	C2	Tryptophan-like	Au ^{1,9} , M ⁸

^a T: Terrestrial inputs; Au: Autochthonous primary production; An: Anthropogenic origin; M: Microbial degradation; P: Photochemical degradation.

1) Massicotte and Frenette (2011); 2) Walker et al. (2013); 3) Kothawala et al. (2014); 4) Kellerman et al. (2015); 5) Yamashita et al. (2010); 6) Cawley et al. (2012); 7) Zürbrugg et al. (2013); 8) Stedmon and Markager (2005); 9) Yamashita et al. (2008); 10) Jørgensen et al. (2011).

761

762

763 **Table 2** – Temporal variations of DOM properties measured at the outlet of the Kariba Reservoir during a one year and half
 764 monthly sampling (from February 2012 to November 2013).

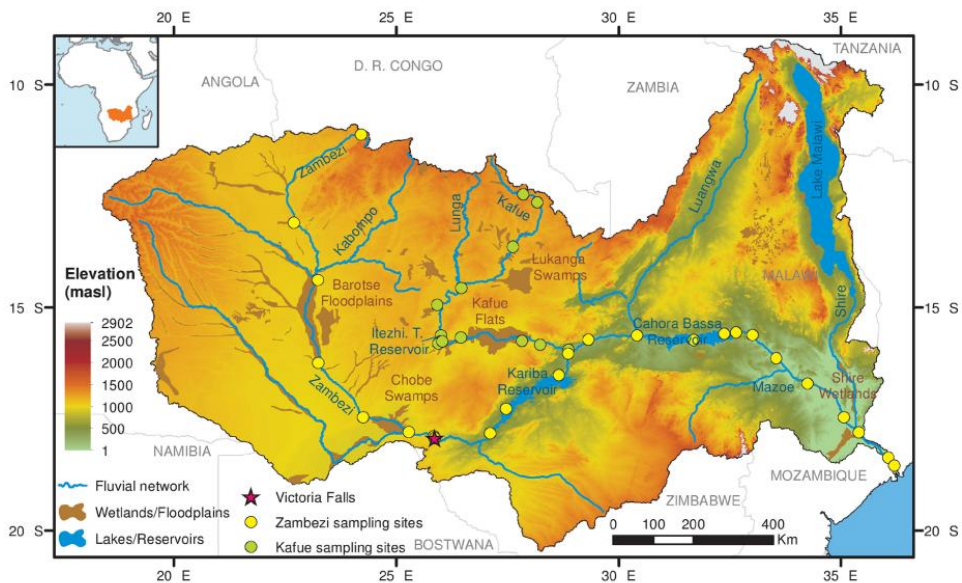
	DOC (mg L ⁻¹)	$\delta^{13}\text{C}_{\text{DOC}}$ (‰)	a_{350} (m ⁻¹)	SUVA ₂₅₄ (L mgC ⁻¹ m ⁻¹)	S _R	%C1	%C2	%C3	%C4	%C5
Min	2,00	-23,96	1,00	1,39	1,010	27,7	12,2	16,1	4,0	12,3
Max	2,60	-22,26	2,50	3,11	1,428	36,5	16,6	26,2	13,8	35,9
Mean	2,22	-23,08	1,60	2,02	1,185	34,1	15,2	24,1	9,3	17,3
S.D.	0,17	0,37	0,44	0,43	0,141	2,4	1,2	2,7	3,1	6,2
<i>n</i>	20	20	12	12	12	12	12	12	12	12

765



766 **Figure 1**

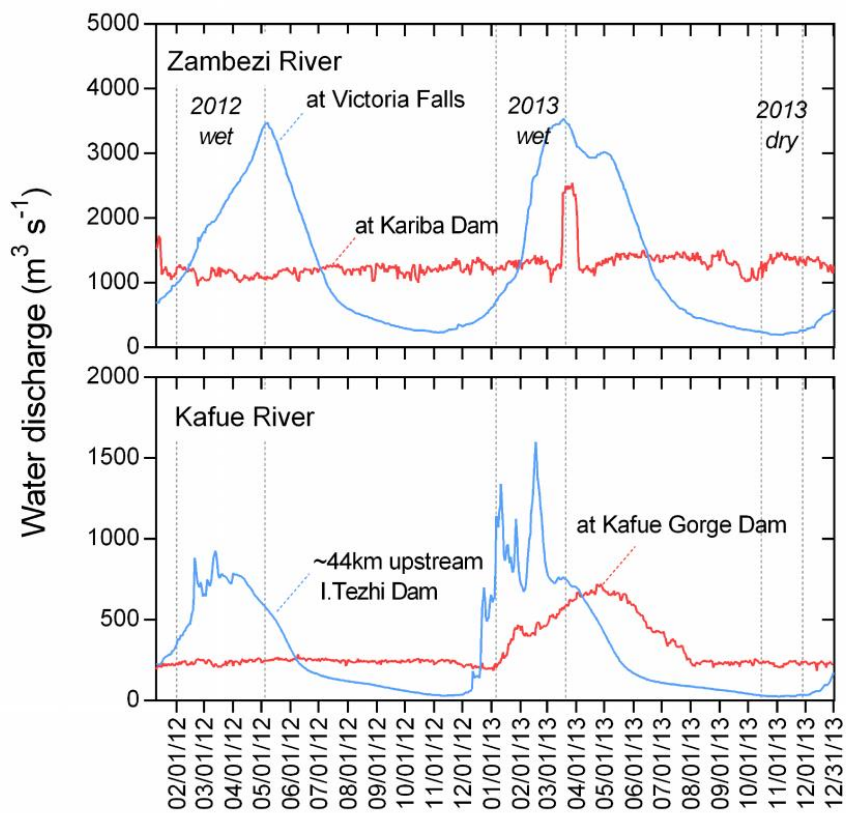
767



768



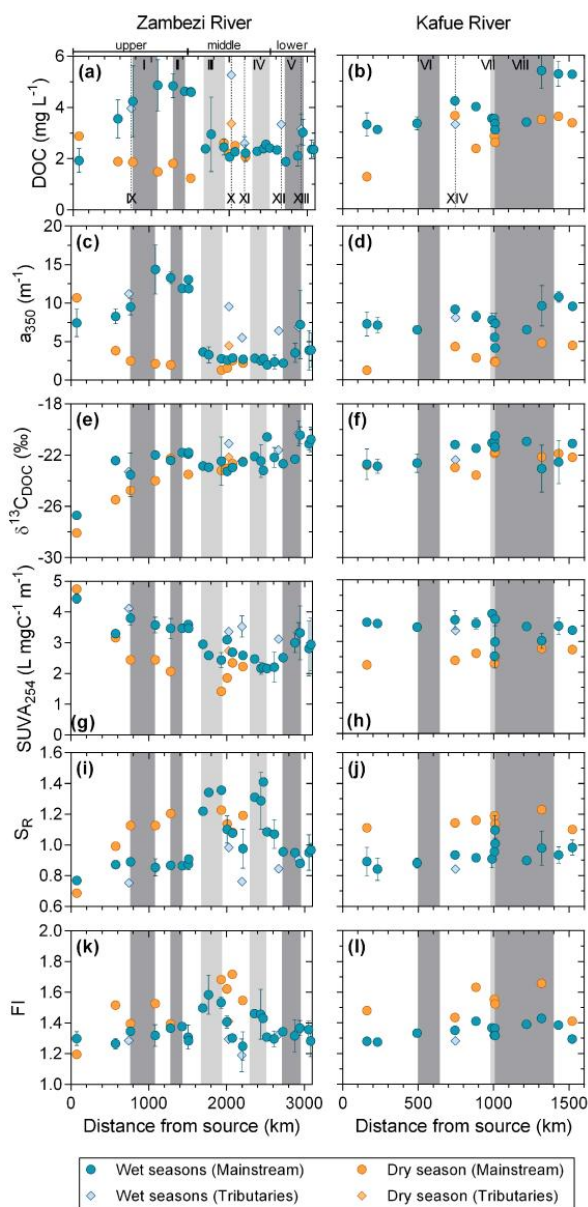
769 **Figure 2**



770



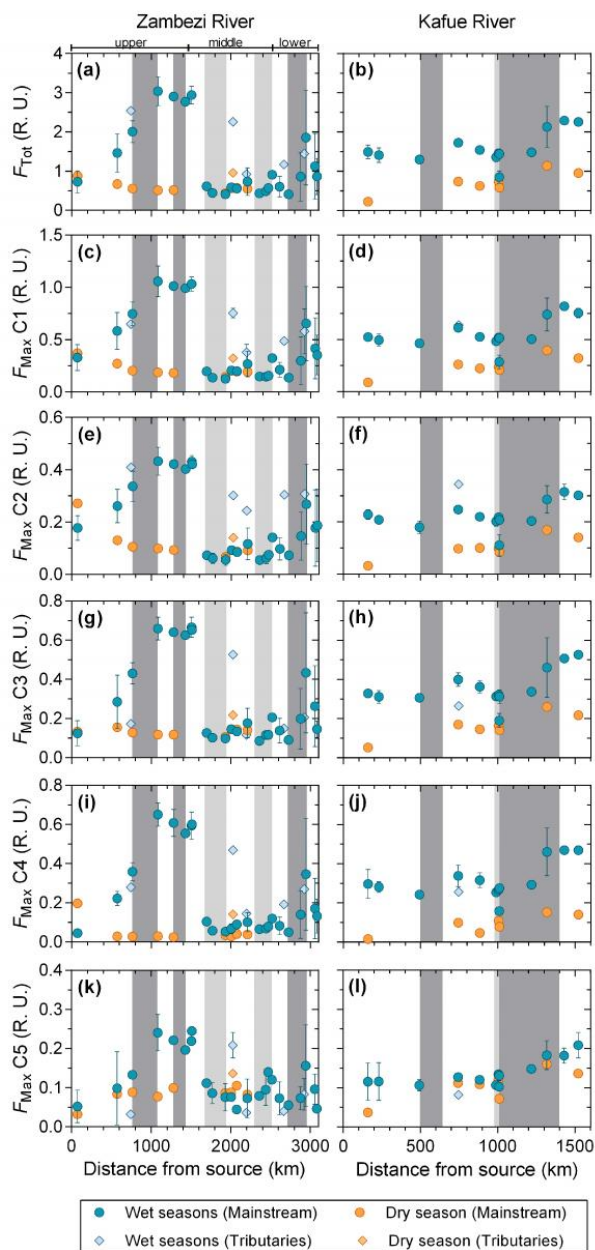
771 **Figure 3**



772



773 **Figure 4**

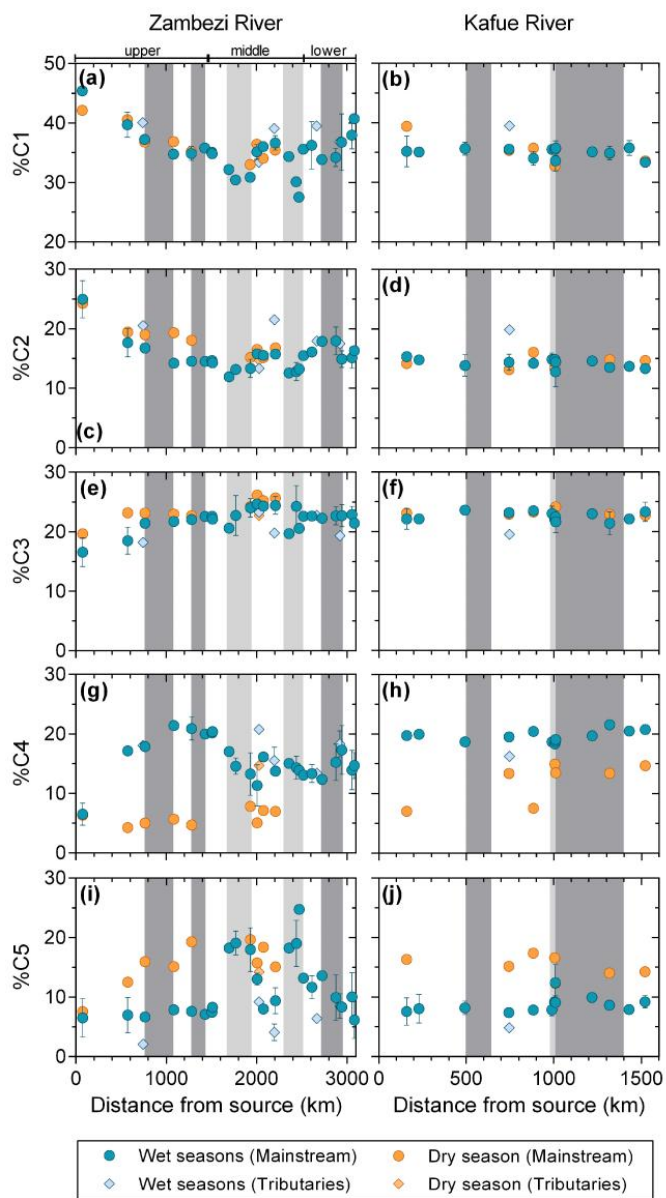


774

38



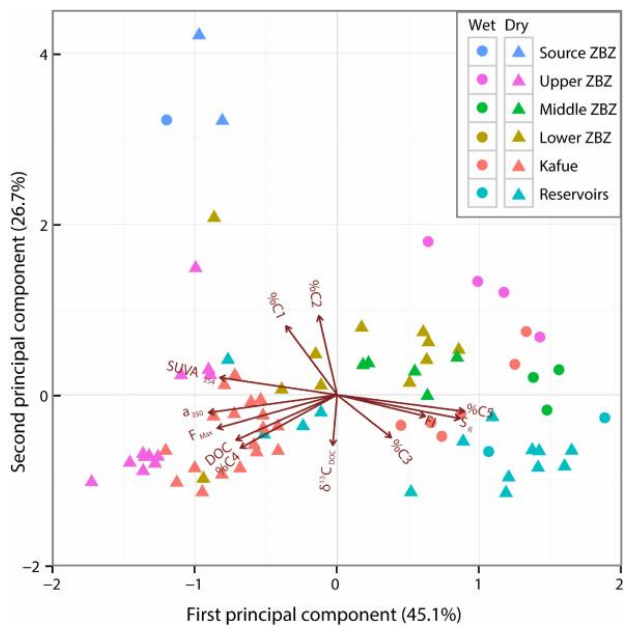
775 **Figure 5**



776



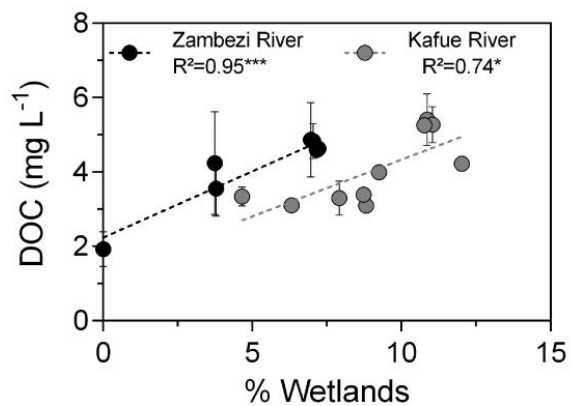
777 **Figure 6**





779 **Figure 7**

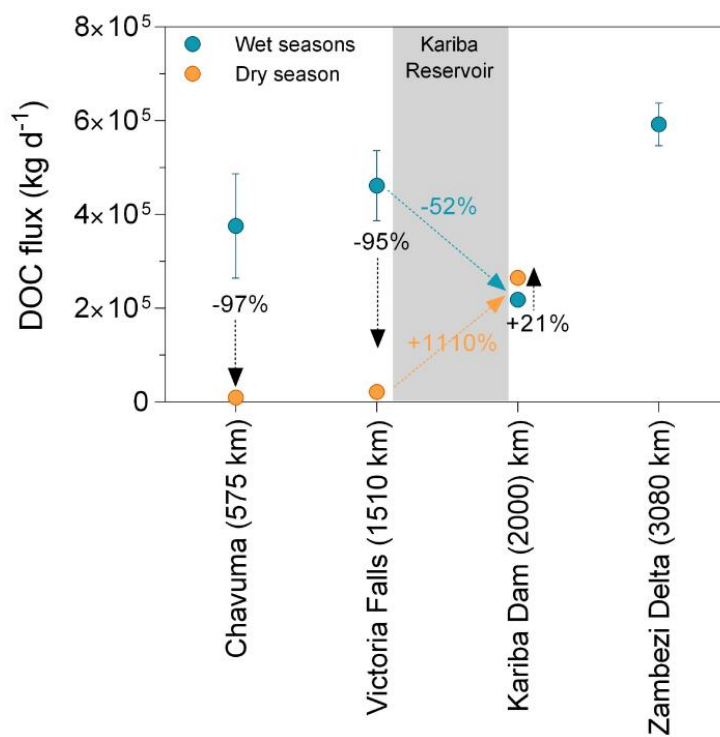
780



781



782 **Figure8**



783

784

785

786